Predictive microbial community changes across a temperature gradient

Keywords: Community assembly, temperature, microbial ecology, metabolism, thermal performance, physiology.

Xin Sun[1,2,3,*], Jacquelyn Folmar[1], Ariel Favier[4], Nora Pyenson[1], Alvaro Sanchez[1,5], María Rebolleda-Gomez[1,2,4,*]

Abstract

A central challenge in community ecology is predicting the effects of abiotic factors on community assembly. In particular, microbial communities play a central role in the ecosystem, but we do not understand how changing factors like temperature are going to affect community composition or function. One of the challenges is that we do not understand the mechanistic impacts of temperature on different metabolic strategies, nor how this metabolic plasticity could impact microbial interactions. Dissecting the contribution of environmental factors on microbial interactions in natural ecosystems is hindered by our understanding of microbial physiology and our ability to disentangle interactions from sequencing data. Studying the self-assembly of multiple communities in synthetic environments, here we are able to predict changes in microbial community composition based on metabolic responses of each functional group along a temperature gradient. This research highlights the importance of metabolic plasticity and metabolic trade-offs in predicting species interactions and community dynamics across abiotic gradients.

Introduction

We currently live in times of rapid change and unprecedented anthropogenic disturbances, making it paramount to understand and predict microbial changes in response to external stressors. Microbial communities break down organic matter and engage in multitrophic interactions (Solden et al. 2018; Pontrelli et al. 2022; Glassman et al. 2018), directly impacting biogeochemical cycles and primary productivity (Nguyen et al. 2022; Kim et al. 2023; Schlesinger and Andrews 2000). Changes in microbial communities' composition can drastically alter their function, leading to consequences at the ecosystem level (Glassman et al. 2018; Cavigelli and Robertson 2000; Reed and Martiny 2013; Matulich and Martiny 2015).

Forecasting changes in biological communities is a central goal in ecology, yet the complexity of these communities makes this a challenging task. Changes in the environment affect the physiology of individual organisms and interactions between them, leading to changes in the composition and function of biological communities (Dell, Pawar, and Savage 2014; Burnside et al. 2014; Crocker et al. 2023; D. J. Smith and Amarasekare 2018; Amarasekare 2015). These changes in communities generate feedback loops between the biological systems and their abiotic environment, resulting in further shifts in both systems (Suding, Gross, and Houseman 2004; García et al. 2023; Tseng, Bernhardt, and Chila 2019). One way of overcoming these challenges is through the integration of organismal physiology in predicting population dynamics (Brown et al. 2004; Savage et al. 2004).

Temperature is one of the most important abiotic factors structuring past and present ecological communities and their interactions (e.g. Swain et al, this special section). In particular, increased temperatures have a large impact on microbial communities across different ecosystems (Thomas et al. 2012; Wu et al. 2022). Temperature changes affect bacterial physiology (Price and Sowers 2004; Allison et al. 2018; Postmus et al. 2008), species interactions (Amarasekare 2015; Dziallas and Grossart 2012), and therefore community function (Allison, Wallenstein, and Bradford 2010; Xiao et al. 2023; Hall and Cotner 2007). Warming promotes the growth of heterotrophic microbes and accelerates their metabolic

rates, which may result in a larger CO_2 flux– creating a positive feedback between warming and elevated CO_2 (Davidson and Janssens 2006; Frey et al. 2013). However, the effects of temperature on carbon fluxes depend on (among other things) microbial physiology and community composition (Allison, Wallenstein, and Bradford 2010; Auffret et al. 2016). Thus, it remains unclear how community structure and function will change with increasing temperature. To better forecast (and potentially intervene) we require a better integration of cellular physiology in our understanding of ecological dynamics.

Recent work in microbial ecology has shown that similar environments favor similar functional groups, despite substantial variation at lower taxonomic levels (Louca et al. 2018; Goldford et al. 2018). The simultaneous observation of functional convergence and taxonomic divergence has been explained using synthetic communities, but the impact of different abiotic factors on community assembly remains poorly understood. Replicated community assembly in synthetic habitats with a single limiting carbon source led to reproducible assemblies at the family level (Goldford et al. 2018). These assemblies vary across carbon sources, but similar carbon sources result in similar communities (Estrela et al. 2021). In particular, community assembly in sugars can be described by simple metabolic rules.

Structure in these communities results from a couple of metabolic trade-offs. First, heterotrophic bacteria tend to specialize along an axis of sugar–organic acid preference (Gralka, Pollak, and Cordero 2022). The dominant families in these communities differ in their specialization: fermenter taxa (often of the Enterobacteriaceae family) prefer sugars, whereas respirators (members of Pseudomonadaceae and Moraxelaceae families) grow better in organic acids (Estrela et al. 2022). This specialization makes sense because there is a cost of switching between tasks (Goldsby et al. 2012); there is a trade-off between growth at one of these carbon sources and the time it takes to switch to the other one (Basan et al. 2020). The second trade-off is between fermenters' growth rate and yield. Respirofermentative bacteria can both ferment or respire sugars. As their growth rate increases, they start fermenting more, decreasing their ATP yield and secreting more organic acids into the media (Basan et al. 2015;

88 Thomas Pfeiffer and Bonhoeffer 2002). These two trade-offs are enough to quantitatively
89 predict the ratio of respirator to fermenter taxa (R/F) in these communities (Estrela et al. 2022).
90
91 The predictability of community function in these communities and the ability to
92 monitor and control ecological processes in their synthetic habitats make them an ideal model
93 system to evaluate the impact of different abiotic factors on species interactions and
94 community assembly (Estrela, Sánchez, and Rebolleda-Gómez 2021; Sun and Sanchez 2023).
95 In particular, temperature is rapidly changing and it is an environmental factor central to
96 determining microbial community structure and function (Abreu et al. 2023; Sheik et al. 2011;
97 DeAngelis et al. 2015), but its multifaceted impacts on microbial physiology and interactions
98 make it challenging to predict its consequences on microbial communities.
99 We hypothesized that as temperature increases we would see an increase in growth
100 rate at the expense of biomass formation, as respiro-fermentative bacteria switch from a more
101 carbon-efficient but slower-growing respirative metabolism to a faster-growing but inefficient
102 fermentatative strategy (T. Pfeiffer, Schuster, and Bonhoeffer 2001). As a consequence, we
103 would expect more organic acid secretions favoring the growth of respirators (Estrela et al.
104 2022; Basan et al. 2020; Schink et al. 2022), which should result in an increase in R/F at the
105 community level with increasing temperatures. If our hypothesis is correct, we should be able
106 to predict changes in community composition across a temperature gradient.
107
108 **Methods**
109 ***Microbial communities enriched in defined media with different carbon sources across a***
110 ***temperature gradient***
111 To get a diverse community of microbes as a source, we collected ~1.5 g leaf litter from White
112 Oak (*Quercus alba*) trees at Yale West Campus (41°15′27′′N, 72°59′34′′). The temperature at
113 the time of sampling was 25°C. To create the inoculum, we added phosphate-buffered saline
114 (PBS) to reach a final volume of ~15 mL; we incubated the leaf sample for two days at room
115 temperature vortexing the sample every day for 1 minute release the cells from the leaf. We let
116 the leaves settle at the bottom and used the top liquid to inoculate 96 wells of five different

117 deep-well plates (one per temperature). In each plate, we had wells with 500 μL of M9 minimal
118 medium with one of 23 carbon sources (see Table S1). Each carbon source had the same
119 concentration of carbon (0.07 C-mol/L). For each carbon source, we had four replicate wells.
120 In addition, we had 4 wells with M9 and water as the control. In this paper, we are only
121 examining the communities assembled in sugars (Table S1).
122 In the first two transfers, we added a final concentration of 200μg/ml of cycloheximide
123 to exclude eukaryotic cells from our experiment (as in (Goldford et al. 2018)). We incubated
124 each plate at a different temperature (12°C, 22°C, 30°C, 37°C, and 42°C) in different
125 incubators. To control for variation in incubator conditions, we maintained our cultures at high
126 relative humidity in big plastic containers inside each incubator. We tracked humidity and
127 temperature conditions throughout the experiment with Track-It RH/Temp data loggers
128 (Monarch instrument, NH, USA; Figure S1). We checked periodically to make sure that
129 conditions were being maintained. The first 3 days, the 37°C treatment had consistently higher
130 temperatures, between 38-39°C so we adjusted the settings in the incubator. Afterwards, it
131 maintained a mean temperature of 37.7°C and a standard deviation of 0.15°C (excluding door
132 openings). We kept the plates with new media at the appropriate temperature for at least one
133 hour before the transfer to avoid large fluctuations in temperature.
134
135 After 48 hours of growth, we transferred 4 μL of each culture into 496 μL of fresh M9
136 media with the corresponding carbon source. We performed a total of 18 transfers to let the
137 communities stabilize. We measured the optical density at a wavelength of 620nm (OD620) of
138 each culture by sampling 100 μL cultures after each 48-hour growth cycle, and we stored the
139 remaining cultures with a final concentration of 40% glycerol at -80°C. In previous work, we
140 have seen that at 30°C twelve transfers are enough to allow communities to assemble into a
141 generational equilibrium, where the community composition at the end of the batch
142 incubation is maintained in subsequent incubations (Goldford et al. 2018). In this case, we
143 allowed for 50% more passages to account for differences in growth rates across temperatures.
144
145

146 ***DNA extraction and 16S rRNA gene sequencing***

147 We extracted DNA from communities stored in 40% glycerol at -80°C after the last transfer. We
148 let the plates completely thaw to remove the glycerol; we centrifuged the plates to pellet all
149 the cells, and carefully removed all the supernatant. Then we re-suspended the cells in 180µl
150 of enzymatic lysis buffer (20 mM Tris-HCl, 2mM sodium EDTA, 1.2% Triton X-100), we added
151 20 mg/mL of lysozyme from chicken egg white (Sigma-Aldrich) and incubated the mix at 37 °C
152 for 30 min with gentle shaking (200rpm). To lyse the cells, we added 5µl of proteinase K and
153 200µl of buffer AL (Qiagen). We mixed the samples and incubated them for 1 hr at 56 °C.
154 Following cell lysis, we extracted the DNA of all of these samples using the DNEasy Blood and
155 Tissue kit (Qiagen) as described in the protocol. We stored the extracted DNA at -20 °C before
156 shipping it in dry ice for sequencing. For sequencing, the 16S rRNA amplicon library was
157 prepared as described in the Earth Microbiome Project Protocol
158 (http://www.earthmicrobiome.org/protocols-and-standards/16s/). Briefly, the PCR-amplified
159 libraries were prepared using the primer pair F515/R806. Then, the generated amplicons
160 (spanning the V4 region of the 16S rRNA gene) were pooled and sequenced in paired-end
161 reads using the Illumina MiSeq platform (Caporaso et al. 2012). All sequencing procedures
162 including the library preparation were performed at the Argonne National Laboratory (Lemont,
163 IL). Short-read sequences are available in the NCBI SRA, accession number (PRJNA992630).
164

165 ***16S sequencing data analysis***

166 The first step to analyzing our 16S amplicon data was to demultiplex the file using *idemp* a
167 custom script by Yinghua Wu (https://github.com/yhwu/idemp). We then used the pipeline
168 from dada2 version 3.16 (Callahan et al. 2016). Briefly, we first filtered and trimmed reads
169 according to their overall quality profiles. We trimmed the reads after 230bp for both forward
170 and reverse reads or, if the quality was too low, after the first instance of a quality score less or
171 equal to 11. After trimming forward reads with more than 1 "expected error" (EE) and reverse
172 reads with more than 2 were discarded. DADA2 calculates expected errors based on the
173 quality score Q, as $EE = \Sigma(10^{-Q/10})$. Next, reads were de-replicated and merged. At this point
174 reads should be ~250bp, we removed reads longer than 256bp (0.17%). There were no reads

175 shorter than 248. We also removed chimeras. After the whole process, we ended up with a
176 median of 50,000 reads per sample (Figure S2). We assign taxonomy using the Silva database
177 (version 132) using the RDP classifier (Wang et al. 2007) as implemented in DADA2. For all
178 downstream analyses, we rarefied our data at the minimum number of reads per sample (8064)
179 using the R package vegan (Oksanen et al. 2007).
180
181 ***Respirator to fermenter ratio estimation***
182 To estimate the R/F (respirator to fermenter) ratio from 16S data, we assigned members of the
183 Enterobacteriaceae, Enterococcaceae, and Lachnospiraceae families to fermenters, and
184 Pseudomonadaceae, Burkholderiaceae, Rhizobiaceae, Moraxellaceae, and
185 Xanthomonadaceae to respirators according to the literature (Table S2). In previous work, we
186 have confirmed the functional role of Enterobacteriaceae and Pseudomonadaceae, the two
187 dominant families in our communities (Estrela et al. 2022). In addition, all of the fermenter
188 isolates from this work (family Enterobacteriaceae) produced organic acids when grown in
189 glucose confirming their fermentation ability.
190
191 ***Isolation of strains from enrichment communities***
192 To evaluate the role of thermal responses of individual isolates in predicting community
193 assembly, we isolated strains from microbial communities stabilized in media with one of four
194 sugars (glucose, fructose, galactose, ribose) at five different temperatures. We thawed the
195 microbial communities from the last transfer stored at -80°C. After making sure that these
196 communities were well mixed, we took a small sample diluted and plated it in chromogenic
197 agar (Universal Chromoselect, Sigma Aldrich). Chromogenic agar allowed us to distinguish our
198 fermenter taxa (blue, purple, and pink colors) from groups of respirators (white colonies). We
199 selected two different colonies of each group per carbon source and temperature. In some
200 cases, we were not able to isolate respirators because there were none on agar plates. We
201 streaked each isolate and picked a single colony each time to remove possible contamination,
202 we repeated this streaking at least two times per isolate. We inoculated a single colony of each
203 of these isolates in a different well of a 96-deep-well plate with 500 µL of trypticase soy broth

204 (TSB) media on each well. We let these isolates grow for 24hrs at 30°C. We stored the isolates
205 in 40% glycerol at -80°C for further analyses. We confirmed our functional assignment by
206 identifying each isolate through Sanger sequencing. Before all phenotypic measures, we
207 plated all isolates to check for contamination and confirm their identity.
208
209 To evaluate how well our isolates represented the communities, we aligned the Sanger
210 sequences of our isolates to amplicon sequencing reads (ESVs) of the communities as
211 described in (Estrela et al. 2022). We performed a pairwise alignment between Sanger
212 sequences and all ESVs from the same community, the alignment with the highest alignment
213 score was picked with zero or one base pair mismatch. In general, our isolates represented
214 their source communities well with an average coverage of 84.4% for replicate community 2
215 and 81.2%for replicate community 4 (Figure S3).
216
217 ***Measurement of growth curves of strains***
218 We performed growth assays with isolates under 12°C, 22°C, 30°C, 37°C, and 42°C. To
219 acclimate the strains before growth assays, we grew isolates from glycerol stocks in 500 μL
220 trypticase soy broth (rich media) in 96 deep-well plates for 24 hours in incubators with desired
221 temperatures. We transferred 5 μL of these cultures to 200 μL fresh M9 media with one of the
222 four carbon sources (glucose, galactose, fructose, and ribose) in 96-well NUNC plates. Medium
223 with each carbon source had three replicates for experiments performed at 12°C, 22°C, and
224 30°C. One plate was made for each carbon source at 37°C and 42°C. After incubating 12 or 4
225 plates for 48 hours under desired temperatures, we measured OD values for grown cultures.
226 Then, we transferred 4 μL of grown cultures to 200 μL fresh media. We used a plate reader
227 (Biotek Epoch 2) with a microplate stacker (BioStack 4) to measure the growth curve for each
228 isolate over the course of 48 hours in a temperature-controlled room set at 12°C, 22°C, or 30°C.
229 The highest temperature for the temperature-controlled room was 30°C, so we measured the
230 growth curve of isolates in four carbon sources in four plate readers set at 37°C or 42°C
231 (accuSkan FC). To make sure there were no significant effects of plate reader in our growth
232 measurements we compared data from both plate readers for plates at 30°C (Figure S4).

233

234 To determine growth parameters (lag phase, maximum growth rate) we used a custom
235 function that fits a generalized additive model (gam) to the ln(OD620) value over time using a
236 penalized cubic regression spline (bs=cs) using the gam function from the mgcv package
237 (Wood 2011) in R version 4.2.2 (R Core Team 2023). These are very flexible models that allow
238 us to track different moments in these curves accurately. The cubic spline penalty minimizes
239 problems with noise and overfitting while still closely following the dynamics of otical density
240 over time. Our function then approximates the derivative for the predicted values at each point
241 using a finite difference interval ($1 * 10^{-5}$). The maximum growth rate is calculated as the
242 maximum derivative after filtering initial values (first two hours) because at this point noise is
243 large in proportion to the signal leading to spurious values of maximum growth rate.

244

245 To fit thermal performance curves, we used a Gaussian response to temperature,
246 where:

247 $$r(T) = r_{max}\, e^{-0.5\left(\frac{(T-T_{opt})^2}{\alpha}\right)}$$

248 describes growth rate at a given temperature (*r(T)*) as a function of the maximum growth rate
249 at the optimum temperature (T_{opt}), the current temperature (T) in reference to the optimum,
250 and a value of thermal breath (α) (Lynch and Gabriel 1987; Amarasekare 2015). From our fit we
251 estimated the values of T_{opt}, rmax, and α. We used the rTPC pipeline in R to fit this model to
252 our data (Padfield, O'Sullivan, and Pawar 2021).

253

254 ***Measurement of organic acid secretion by fermenters***

255 We streaked isolates stored in 40% glycerol on chromogenic agar plates to check for
256 contamination. After incubating the plates for one day in a 30°C incubator, we picked a single
257 colony for each isolate and resuspended it in 200 µL PBS in a 96-deep-well plate. Then, we
258 transferred 5 µL of these inocula into 500 µL fresh M9 media with glucose in five 96 deep-well
259 plates. We incubated each plate under one of the five temperatures (12°C, 22°C, 30°C, 37°C,
260 and 42°C). After two days, we transferred 5 µL cultures from each deep-well plate to 500 µL

261 fresh M9 media with glucose in two replicate 96-well NUNC plates for destructive sampling at
262 two time points. For temperature 12°C, we sample after 24 hours (T1) and 48 hours (T2). For
263 the other four temperatures, we sacrifice one replicate plate after 12 hours (T1) and the other
264 after 24 hours (T2). T1 is within the exponential phase of most cultures and T2 is a time when,
265 on average, the population has reached carrying capacity in glucose, but bacteria have not
266 switched to start consuming organic acids (Figure S5) (Estrela et al. 2022).
267
268 At each time point, we sampled 100 μL of culture to measure OD (620 nm). We
269 centrifuged the rest of each culture at 3600 rpm for 25 minutes to separate cells and their
270 supernatant. After centrifugation, we carefully transferred 200 μL of supernatant into 96-well
271 plate filters and collected the supernatant into 96-well NUNC plates by centrifuging at 3200
272 rpm for 10 minutes. We stored the supernatant plates at -20°C until analysis. To obtain per
273 capita organic acid production, and estimate yield, at T2, we streaked cultures from selected
274 wells with fermenters on chromogenic agar plates for colony counting. We estimated all
275 fermenter cell numbers at T2 by measuring OD (620 nm) values and the linear regression
276 between colony numbers and OD (620 nm) values of selected wells (R^2=0.939).
277
278 We used colorimetric methods to measure acetate and lactate concentrations in wells
279 with fermenters based on the manufacturer protocols (abcam ab204719 for acetate, abcam
280 ab83429 for lactate). We diluted samples to the range of the standard curve. We made two
281 standard curves with identical standard dilutions for each batch of samples to cover variations
282 among kits. We calculated final concentrations based on the sample dilution rate and the
283 standard curve, a linear regression between measured OD (450 nm) and acetate amount of
284 the corresponding standard.
285
286 ***Measurement of glucose consumption***
287 We measured the glucose consumption of all isolates across conditions using a Glucose (GO)
288 Assay Kit (Sigma-Aldrich). First, we obtained 200μL of the supernatant at the endpoint by
289 centrifuging at 3200 rpm for 10 mins using filter plates (Pall Acroprep, supor filter plate

290 0.25μm). Afterward, we prepared a glucose standard curve as specified by the assay kit (with
291 a working range of 20 - 80 ug/mL), and we diluted the supernatants accordingly. Using a 96-
292 well pipettor to minimize variation in reaction time, we added 20 uL of the dilutions and
293 standards to another 96-well plate containing 40 uL of a colorimetric assay reagent. We
294 incubated the plate at 37°C for 30 min. We carried out all the steps in complete darkness. We
295 finally interrupted the reaction by adding 40 uL of 6N H2SO4 and measured the absorbance
296 at 540 nm (Multiskan FC, Thermo Fisher Scientific). We calculated the absolute glucose
297 consumption, as well as the percentage of glucose consumption based on the M9 medium
298 (0.21% Glucose).
299
300 ***Calculation of glucose efficiency***
301 In previous work we proposed a model to describe the dynamics of these communities and
302 quantitatively predict the ratio of respirators to fermenters, R/F (Estrela et al. 2022). Assuming
303 that glucose is only consumed by fermenters (F) and the organic acids are only consumed by
304 the respirators (R), we can approximate R/F as:
305
$$\frac{R}{F} \approx D_{oa,glu} \frac{w_{oa,R}}{w_{glu,F}}$$
306 Where $w_{glu,F}$ is the yield efficiency of fermenters in glucose, $w_{oa,R}$ is the yield efficiency of
307 respirators in organic acids, and $D_{oa,glu}$ is the number of acetate molecules that fermenters
308 secrete back into the environment per molecule of glucose consumed. Thus, assuming that all
309 carbon uptaken by *F* is either converted to biomass or secreted as organic acids, $D_{oa,glu}$ gives
310 an idea of *F* carbon efficiency. A high value of $D_{oa,glu}$ means that most of the glucose uptake
311 by *F* is secreted back to the media and therefore is no longer available for *F* biomass.
312 These assumptions are justified by a growth advantage of *F* over *R* in sugars and of *R*
313 over *F* in organic acids, as well as the observation that *F* does not co-utilize sugars and acetate,
314 instead switching between these carbon sources requires a shift from a glycolytic direction of
315 central metabolism to a gluconeogenic direction leading to long lag times (Basan et al. 2020;
316 Schink et al. 2022). In addition, in this work, we assume that organic acids comprise only lactate
317 and acetate. These are the dominant carbon sources present in our communities (Estrela et al.

318 2022) and bacteria with a glycolytic preference (F) take a long time to switch and consume
319 both of these carbon sources (Basan et al. 2020).
320
321 We obtained the empirical values of glucose efficiency ($D_{oa,glu}$) at all experimental
322 temperatures by dividing the total carbon consumed as glucose by our fermenter isolates over
323 the total carbon secreted as organic acids by the same fermenters. Glucose efficiency is then
324 1-$D_{oa,glu}$.
325
326 ***R/F prediction***
327 Using these empirical values of $D_{oa,glu}$ and our model, we can predict R/F. We can calculate
328 empirically the biomass of fermenter taxa produced per carbon in glucose ($w_{glu,F}$), as well as
329 the amount of respirators biomass produced per carbon available as organic acids ($w_{oa,R}$). To
330 obtain $w_{glu,F}$, we obtained the optical density after cultures reached their carrying capacity (the
331 same time at which we measured glucose and organic acids in the supernatant). We removed
332 the blank from those values and then divided it by the amount of carbon consumed in the form
333 of glucose. To avoid artifacts of isolates growing at temperatures different than their original
334 community, we used only the values of isolates growing at the temperature at which they were
335 isolated.
336
337 We determined $w_{oa,R}$ from the optical density of communities assembled in acetate
338 (0.07M of carbon). These communities were composed in their majority by respirator taxa
339 (median respirator relative abundance: 0.97, Q1: 0.75, Q3: 0.99), so we could multiply the
340 optical density by the relative abundance of respirators to get an estimate of overall biomass.
341 Then, we calculated the difference between final and initial densities, and assumed that all of
342 the acetate had been consumed. Thus, we calculated $w_{oa,R}$ as the difference between the final
343 and initial optical densities (the initial optical density is the final optical density divided by
344 dilution factor of 125) divided by the total amount of carbon present in the media as acetate.
345 That is: $w_{oa,R} = (OD_{final} - OD_{initial})/C_{acetate}$.
346

347 Finally, as described in our mode (Estrela et al., 2022), we obtained the predicted values
348 of R/F by dividing the values of $D_{oa,glu}$ for each isolate, by the $w_{glu,F}$ calculated for the same
349 isolate. We then multiplied all of these values by the four possible values of $w_{oa,R}$ (one for each
350 replicated community).
351
352 **Results**
353 ***Community composition changes with temperature in a predictable manner***
354 We collected a diverse microbial community from decomposing leaf litter and used it to
355 inoculate replicate habitats with one out of 16 sugars as the only supplied carbon source. To
356 evaluate how temperature affects community assembly in different sugars, after inoculation,
357 we let the communities stabilize through serial transfers in each carbon source at each of five
358 different temperatures (12.5°C, 22°C, 30°C, 37.7°C, 42°C) (Figure 1A; Methods).
359
360 Within each carbon source and temperature the replicate communities were fairly
361 consistent at the family level (Figure 1B). Moreover, we saw replicable patterns across
362 temperatures for all communities. These communities assembled in different sugars were
363 dominated by fermenter taxa (members of the Enterobacteriaceae family) followed by
364 respirators of Pseudomonadaceae, consistent with previous observations (Figure 1B)
365 (Goldford et al. 2018; Estrela et al. 2022), and, as in previous work, despite replicability at the
366 family level, community assembly showed little convergence at the level of exact sequence
367 variants (ESVs) (pairwise Bray-Curtis distance between replicates: Q1 = 0.097, Median = 0.371,
368 Q3 = 0.53; pairwise Bray-Curtis distance between sugars: Q1 = 0.276, Median = 0.619, Q3 =
369 0.896). This divergence between replicates is highest at 12.5°C and decreases with increasing
370 temperature (Figure 1B, Figure S6).

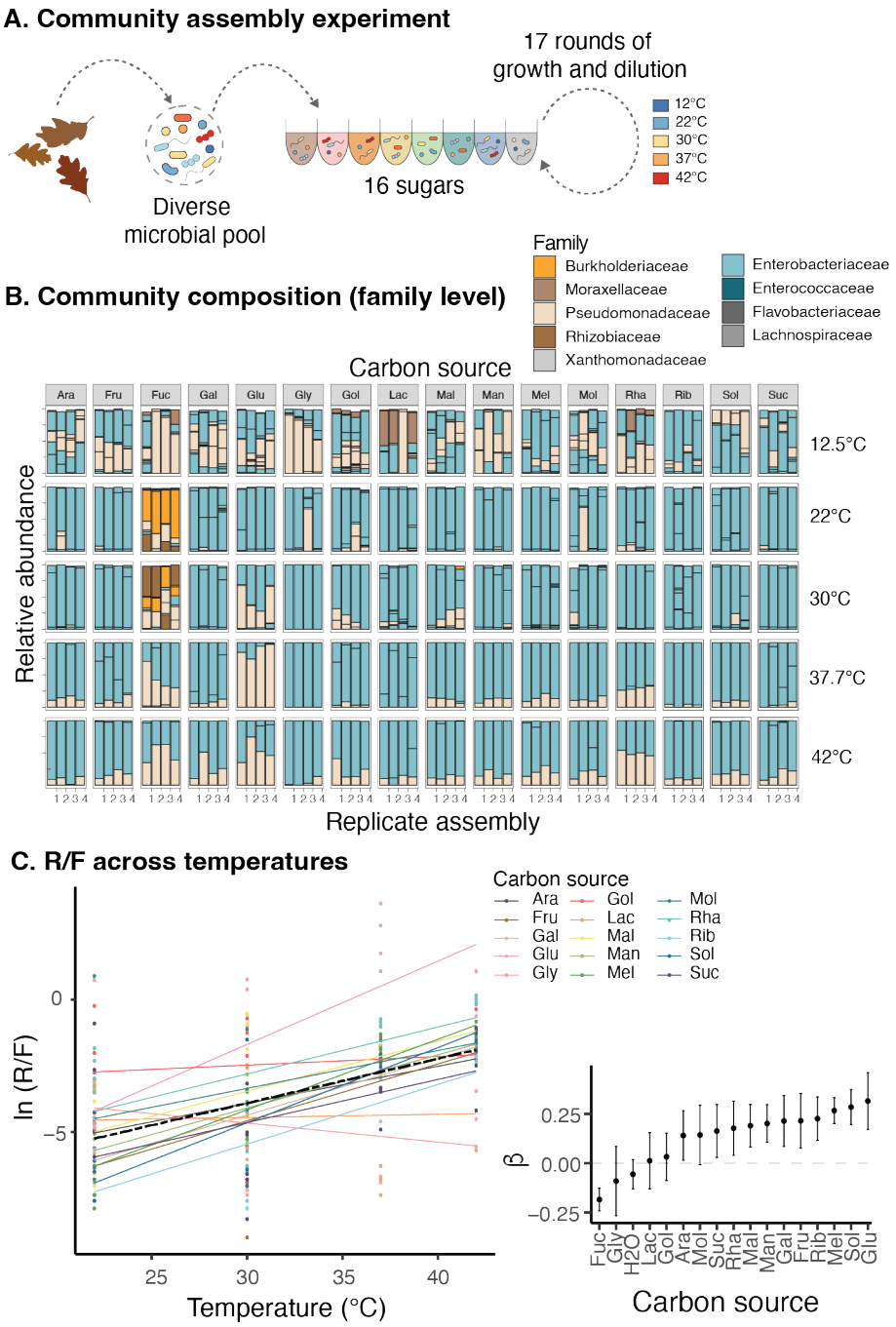

Figure 1. Community assembly experiment. A. Schematic of the protocol. We inoculated different carbon sources with a diverse pool of microbes and let them grow at one of 5 temperatures. B. Relative abundances of different families in each of the communities. The columns are the different sugars and the rows different temperatures of assembly. The 4 bars within the same row and column are replicated assemblies. C. Relationship between temperature (from 22°C to 42°C) and ln(R/F) across the 15 sugars. The dashed line is the mean relationship across carbon sources. Fucose was excluded from this analysis because it had very

distinct dynamics than all of the other sugars. C. Estimates of the slopes (and 95% CI) for the relation between temperature (from 22°C to 42°C) and ln(R/F). Fucose and water are included. We did not observe a significant relationship between temperature and ln(R/F) in communities assembled in water without supplemental carbon sources.

Consistent with our hypotheses, excluding fucose, the respirator to fermenter ratio (R/F) showed an increase with increasing temperatures from 22°C to 42°C (Figure 1C). After log transforming the data, we observed a slight positive relationship between temperature and ln(R/F) (methods; β_1 = 0.17 ± 0.016 SE, p-value < 0.001; Figure 1C). This relationship is maintained for most of the sugars evaluated (Figure 1C, D). Glycerol, galacticol, lactose, arabinose, and sucrose show no clear relationship between temperature and R/F (95% confidence interval of the slope includes 0). Only fucose showed a significant negative relationship between temperature and ln(R/F) (β = -0.184, 95%CI [-2.42, -0.13]). In this sugar we also observed lower optical densities (Figure S7), and overall a much more distinct pattern of assembly (even at the family level) (Figure 1B, D).

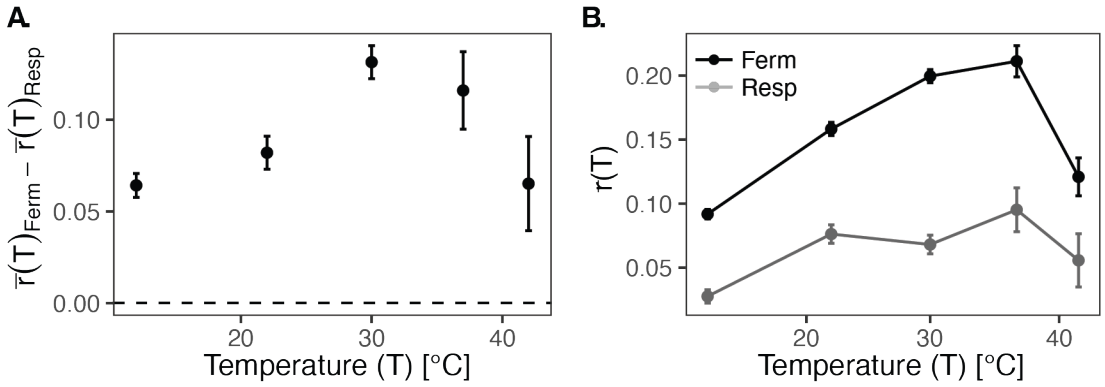

Figure 2. Estimated marginal mean growth rate ($\underline{r}(T)$) after accounting for the temperature of community assembly from which each isolate was taken and the carbon source in which growth was measured. **A.** Difference between the estimated mean growth rate of fermenters and respirators at each temperature. **B.** The estimated mean growth rate of fermenters (ferm) and respirators (resp) at different temperatures. Error bars are the 95% confidence intervals for each estimate.

One possibility that could explain the overall increase in respirators with increased temperatures (after 22°C) is if, in our original inoculum, respirative bacteria had a fitness advantage over fermentors as temperature increases. However, across all temperatures, fermenters tended to grow faster than respirators in the four sugars tested (glucose, fructose, galactose, ribose) (Figure 2, Figure 3A). After controlling for the temperature of isolation and carbon source, the difference in growth fermenters and respirators in the supplied sugars increased approximately 1.6 times between 22°C and 30°C ($\underline{r}(22)_F - \underline{r}(22)_R = 0.082 \pm 0.005SE$ and $\underline{r}(30)_F - \underline{r}(30)_R = 0.131 \pm 0.005SE$; Figure 2), and the R/F ratio for these same carbon sources increased from a mean of 0.012 at 22°C to 0.3 at 30°C.

In contrast, at 12.5°C we observed high diversity, lower replicability between replicates (pairwise Bray-Curtis distance between replicates: Q1 = 0.46, median = 0.501, Q3 = 0.54; Figure S5), and a high R/F ratio across all carbon sources (median = 0.75, Q1 = 0.32, Q3 = 1.47, N = 64). At this temperature the difference in growth between respirators and fermenters is small ($r(T)_F - r(T)_R = 0.064$, 95%CI [0.058, 0.071] ; Figure 2A). As temperatures increase the difference in growth between respirators and fermenters increases to a maximum around 30°C and decreases again afterward, but even at 37.7°C the growth difference between functional groups is almost twice the 12°C value ($r(T)_F - r(T)_R = 0.116$, 95%CI [0.095, 0.137] ; Figure 2A). This difference in growth between fermenters and respirators across temperatures is mostly shaped by changes in growth rates of fermenters across this same temperature gradient (Figure 2B). Respirators growth is low across all temperatures even though it still increases slightly until 37°C and then goes down again at 42°C (Figure 2B).

Community assembly at higher temperatures selects isolates with higher T_{opt}

We observed differences in maximum growth rates across functional groups (fermenters have higher maximum growth rates across carbon sources), as well as differences in maximum growth rate across carbon sources, and the temperature of origin. We also observed a significant interaction between functional group and temperature of origin on maximum growth rates (Table S3; Figure 3A, Figure S7).

The process of community assembly sorted isolates of the same functional groups according to their thermal physiology. That is, strains isolated from communities assembled at lower temperatures tended to have a lower thermal optimum (T_{opt}) than those from communities assembled at higher temperatures (Figure 3). For each degree higher in the temperature at which communities were assembled, fermenter isolates had on average a 1.073°C±0.107SE increase in T_{opt} (with an intercept of -5.12°C; Figure 3B). Respirators had a similar slope (0.756°C±0.123SE; p-value > 0.05) but a larger intercept (Ferm-Resp: 12.626°C±0.123SE, p-value = 0.018; adjusted R^2 = 0.35; Figure 3B).

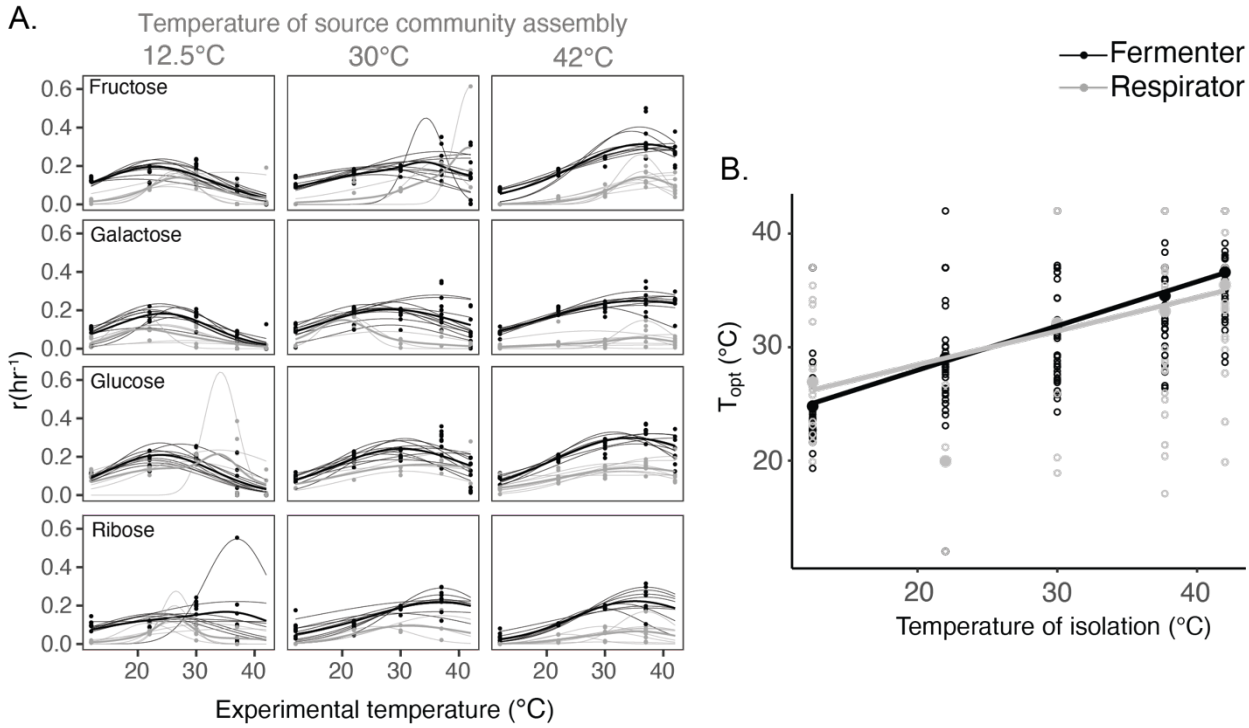

Figure 3. Response of growth rates of fermenters and respirators to increasing temperatures. A. Each column corresponds to a source temperature (the temperature at which the communities were assembled, only 12.5, 30, 42 are shown, all plots are in supplementary), and each row corresponds to the sugar used to measure growth. Each thin line is the Gaussian model fit to one isolate, thick lines are the mean for fermenters (black) and respirators (gray). B. Relationship between the temperature of isolation (the temperature at which the source community was assembled) and the optimal temperature of that isolate (T_{opt}). Outlined small circles are the values of each isolate and filled big circles are the mean value. Lines are the slopes from a linear model.

451 ***Fermenters face a trade-off between growth and glucose efficiency at higher***
452 ***temperatures***

453 We hypothesized that the increase in R/F with temperature is the result of a decrease in
454 metabolic efficiency with faster growth rates (Figure 4A). Fermenters from communities
455 previously assembled in glucose at 30°C showed increased organic acid production at 28 hrs
456 with increased growth rates (slope: 21.67±3.559SE mM secreted to media per hour increase
457 in growth rate; R2 = 0.44, p-value < 0.0001) whereas respirators do not secrete acetate at any
458 growth rate (slope:-0.31±0.45SE mM secreted to media per hour increase in growth rate; R2
459 = 0.03, p-value = 0.5); Figure 4B). Therefore, we expected that increasing growth rates with
460 increasing temperatures would lead to greater amounts of acetate secreted (Figure 4A), but
461 we did not know if different temperatures would have different slopes.
462

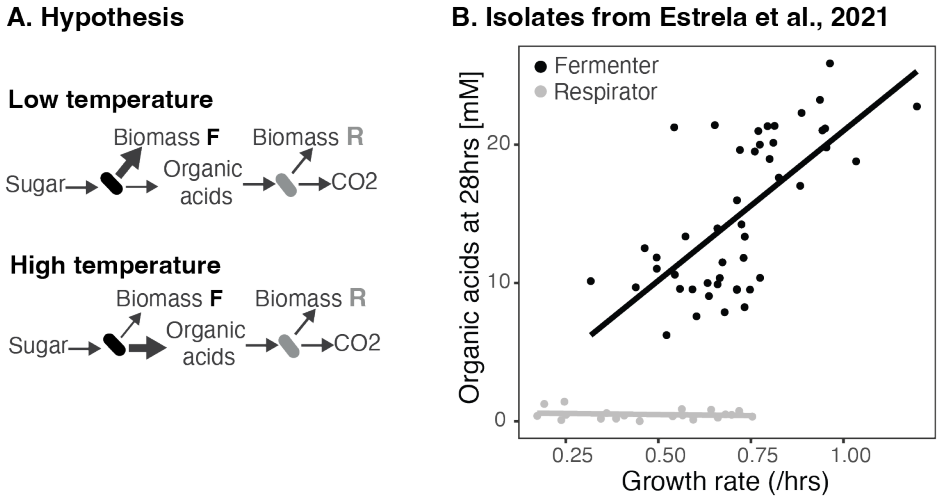

463
464 **Fig 4.** In our conceptual model of interactions between functional groups, fermenters (F)
465 consume sugars and use them for biomass production or secrete them as organic acid waste
466 products into the media. Respirators (R) consume these organic acids and make biomass or
467 produce CO_2. As temperatures increase we expect that fermenters will release more organic
468 acids into the media as a result of their increased growth rate (A). This hypothesis is based on
469 previous data of isolates from communities assembled of glucose at 30°C. Fermenters from
470 these communities secrete an increased concentration of organic acids into the media with
471 increasing growth rates (B).
472
473

474 We grew all isolates in minimal media with glucose and measured the concentration of
475 organic acids (acetate and lactate) produced by the time fermenters reach their carrying
476 capacity (Figure S4). We observed a linear relationship between growth rate and the secretion
477 of organic acids (Figure 5A). For each unit of density (ln(OD600)) per hour faster in growth, we
478 observed an increased total concentration of carbon secreted as organic acids of 68.98± 7.01
479 SE mM (Fig5A;$p < 0.0001$; adjusted $R^2 = 0.31$). This model, however, is obscured by highly
480 variable (and often high) secretions after the T_{opt}. If we remove all points above the T_{opt}, we get
481 carbon secreted as organic acids per hour faster in growth of 96.49± 7.5 SE mM (Figure 5A).
482 The total amount of carbon secreted as organic acids increased with temperature (Figure 5B),
483 reaching a maximum at 37°C and then decreasing at 42°C (after Topt for most isolates). Overall,
484 after 37°C (when most isolates have passed their T_{opt}) secretions stay high for the drastic
485 decrease in growth (Figure 2B; Figure 5A,B).
486

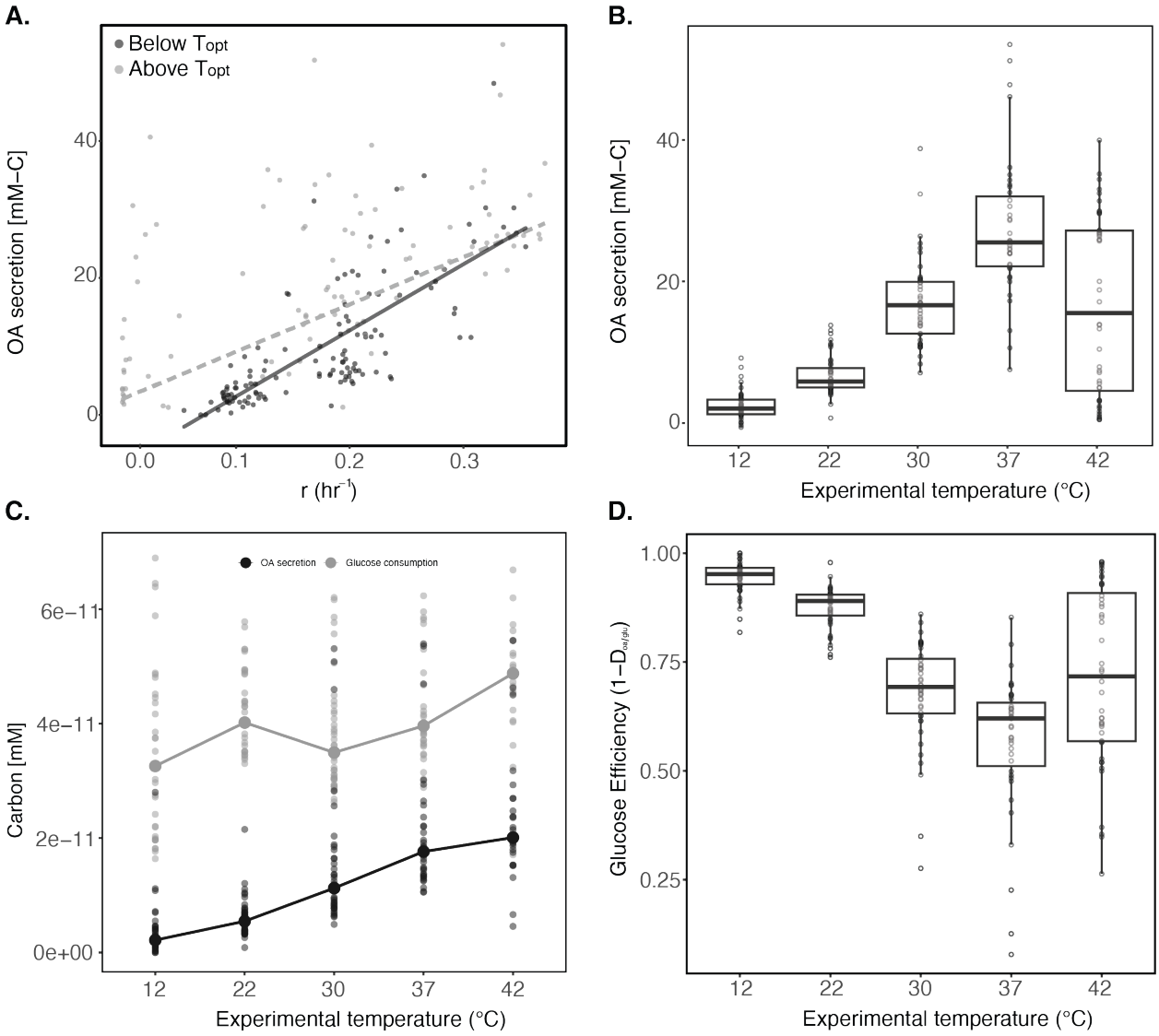

Figure 5. Effect of temperature on the carbon use of fermenters after glucose depletion. **A.** Total carbon that is secreted as organic acids (OA) at different growth rates, with points colored by their experimental temperature above (light) or below (dark) the thermal optimum. Trendlines show linear fits to all data (dashed) and data below the thermal optimum (solid). **B.** Total secreted carbon per temperature. **C.** Consumed and secreted carbon per cell at different temperatures. **D.** Glucose efficiency, calculated as 1 - D oa/glu (ratio of secretions per unit of glucose consumed by fermenter cells), at different temperatures.

The R/F ratio can be quantitatively predicted from a simple model describing the biomass production of fermenters based on the conversion of glucose into biomass by fermenter taxa, and biomass production of respirators from consuming organic acids secreted

499 by fermenters (Figure 4A, Estrela *et al.*, 2021). We wondered if this simple model could also
500 predict the changes in the R/F ratio across a temperature gradient. According to this model
501 carbon from glucose can be utilized for biomass formation of fermenters or released into the
502 media as organic acids. Thus, the fraction of organic acids produced per molecule of glucose
503 ($D_{oa,glu}$) is related to the amount of carbon used in biomass (1-$D_{oa,glu}$) or glucose use efficiency.
504

505 We observed a trade-off between growth rate and glucose efficiency with increasing
506 temperatures leading to faster growth rates at the cost of secreting more organic acids. From
507 glucose consumption and organic acid secretions, we calculated the glucose efficiency (1-
508 $D_{oa,glu}$; see methods). Glucose efficiency decreases with increased temperature and then
509 increases slightly at 42°C (Figure 5D). Glucose efficiency is shaped by secretion of organic
510 acids and a significant increase of glucose consumption per cell at 42°C. While the secretions
511 per cell increase steadily with temperature linear model with temperature of isolation as
512 random factor:5.08 $*10^{-12}\pm$ $1.22*10^{-12}$ mM/(cell*°C), p-value<0.0001; Figure 5C), glucose
513 consumption shows a less clear trend that disappears when removing the 42°C data (linear
514 model with temperature of isolation as random factor: 5.17 $*10^{-11}\pm$ $1.58*10^{-11}$ mM/(cell*°C); p-
515 value=0.0012; removing 42°C data: 1.54 $*10^{-12}\pm$ $2.311*10^{-12}$ mM/(cell*°C); p-value=0.5).
516

517 From 12°C to 37°C, as temperatures increase, we see increased growth rates, a
518 maintenance of glucose consumption (Figure 5C), and an increase in organic secretions per
519 capita. All consistent with a decrease of glucose use efficiency (Figure 5D). In contrast, the
520 seemingly increased in glucose efficiency at 42°C is misleading: there is more glucose
521 consumed per molecule of organic acid secreted, but temperature-induced mortality, also
522 means that there is less biomass sustained. At 42°C most isolates are past their T_{opt} and
523 therefore, for the same growth rate they show a much higher secretion of organic acids (Figure
524 5A; Figure S8). Altogether, these results are consistent with the observed linear increase in R/F
525 ratio with temperature in glucose.
526

527 ***Changes in the fermenter's glucose efficiency predict changes in R/F across***
528 ***temperatures***
529 According to our model (see methods; Estrela et al., 2021), R/F can be predicted from three
530 parameters: the biomass of respirators produced per carbon consumed in organic acids
531 ($w_{oa,R}$), the biomass of fermenters that is produced per carbon in glucose consumed ($w_{glu,F}$),
532 and the amount of carbon as organic acids that is secreted by carbon of glucose consumed
533 ($D_{oa,glu}$). We obtained empirical measurements of $w_{glu,F}$ and $D_{oa,glu}$ from our physiological
534 measurements with fermenters in glucose, and in the absence of empirical measurements of
535 respirators growing in organic acids, we obtained $w_{oa,R}$ from the optical density and relative
536 abundance of respirators in communities assembled in acetate at different temperatures.
537

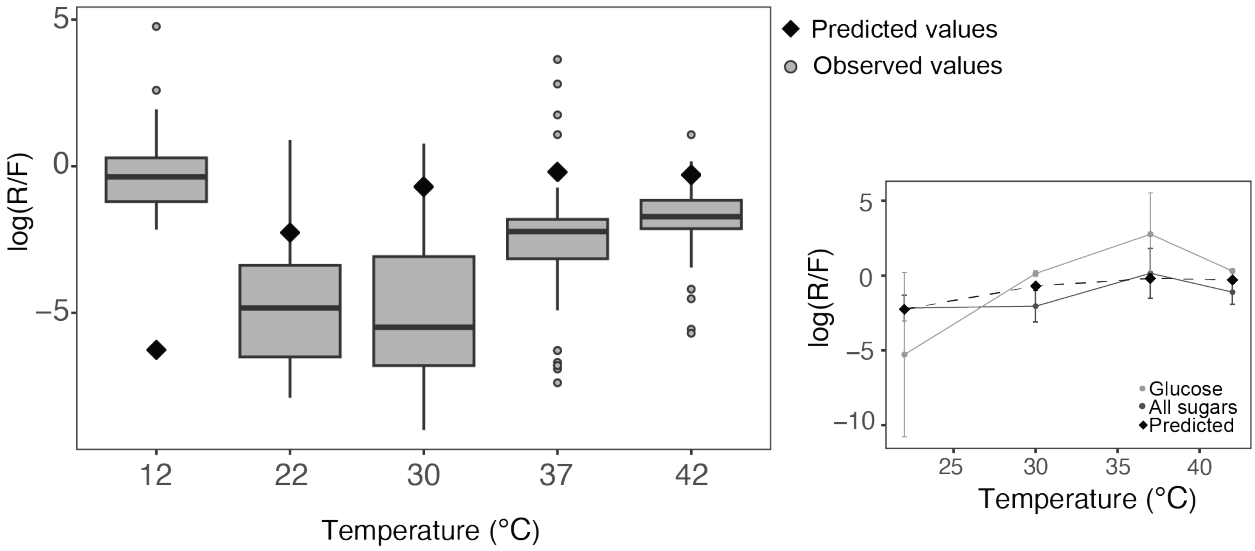

538
539 **Fig 6.** Effect of temperature on the carbon use of fermenters after glucose depletion. **A.** Total
540 carbon secreted as organic acids (OA) at different growth rates, with points colored by their
541 experimental temperature above (light) or below (dark) the thermal optimum. Trendlines show
542 linear fits to data obtained at temperatures above the thermal optimum (dashed) and below
543 (solid). **B.** Total secreted carbon per temperature. **C.** Consumed and secreted carbon per cell
544 at different temperatures. **D.** Glucose efficiency, calculated as 1 - D oa/glu (ratio of secretions
545 per unit of glucose consumed by fermenter cells), at different temperatures.
546
547 Our predicted R/F does not match our observed values at 12°C, given the overall low
548 biomass of respirators and very low $D_{oa,glu}$ we predicted a R/F value of 0.0015 (Q1:0.0009,

549 Q3:0.0024), but overall our communities have a much higher R/F of 0.698 (Q1: 0.299,
550 Q3:1.328). After 12°C we predicted an increase of R/F with temperature until 37°C (Median
551 R/F: 0.714, Q1: 0.707, Q3: 0.903) and then it should be mostly maintained at 42°C (Median
552 R/F: 0.776, Q1: 0.647, Q3:0.828). This is consistent with the behavior of R/F in glucose
553 communities (the sugar we used for our measurements). Quantitatively, however, our
554 predictions tended to overestimate R/F for other sugars, and in the case of glucose, our
555 predicted ratio overestimated the relative abundance of respirators at 22°C and
556 underestimated them at 37°C. Our model accurately predicted R/F of glucose communities at
557 30°C and 42°C (Figure 6). Using coarse measurements of respirator biomass and measuring
558 all parameters from individual isolates (not in a community context) we obtained a prediction
559 that qualitatively follows the dynamics of our communities from 22°C to 42°C, and
560 quantitatively sits in between the observed values for all communities and the ones assembled
561 in glucose.
562
563 **Discussion and conclusions**
564 Microbial communities often show high variation at lower taxonomic levels consistent with
565 significant contributions of stochasticity (Albright, Chase, and Martiny 2019), priority effects
566 (Debray et al. 2022; Chappell et al. 2022), and alternative stable states (Estrela et al. 2022).
567 Nevertheless, these same communities are often remarkably replicable in function (Louca,
568 Parfrey, and Doebeli 2016; Nelson, Martiny, and Martiny 2016; Burke et al. 2011).
569
570 In previous work, we have shown that we can derive simple rules of community
571 assembly and quantitatively predict the relative abundance of different functional groups
572 (fermenters, and respirators) using some basic knowledge about the physiology and
573 metabolism of these groups. In this study, we were able to expand these simple rules to a
574 temperature gradient.
575
576 Consistently with previous work (Basan et al. 2015), we have previously observed that
577 fermenters display a trade-off between growth and yield, increasing their organic acid

578 secretions with increasing growth rates (Estrela et al. 2022). Here, we showed that with
579 increasing growth rates resulting from higher temperatures, there is an increase in organic acid
580 secretions, and therefore a decrease in glucose use efficiency. Overall, this means
581 proportionally more resources available for respirator taxa, and an increase in the ratio of
582 respirators to fermenters (R/F).
583
584 With the exception of communities assembled at 12°C, using physiological data of
585 fermenter isolates growing in glucose, and biomass data from communities assembled in
586 acetate, we were able to predict qualitatively the patterns of change of R/F. Our quantitative
587 predictions tended to overestimate R/F for most carbon sources but performed better for
588 communities assembled in glucose (except the ones at 37°C) where communities in glucose
589 had a really high R/F. Overestimation is to be expected given that our respirator biomass
590 comes from communities starting at high concentrations of acetate. In contrast, in our sugar
591 communities organic acids reach much lower concentrations of organic acids, and only after
592 fermenters have depleted most of the glucose. Thus, and given that growth rate is a saturating
593 function of resource concentration, it would be expected that respirators cannot achieve the
594 same biomass per molecule of organic acid in the sugar communities.
595
596 All of the communities in this study were assembled from the same original pool of
597 species, nevertheless, we observed distinct community composition at the ESV level, even
598 between different replicate assemblies in the same carbon source and at the same
599 temperature. This result indicates a significant contribution of stochasticity in community
600 assembly. Despite stochasticity, we observed functional replicability across communities and
601 a clear effect of selection on community assembly. For example, isolates with different thermal
602 optima were favored at different temperatures.
603
604 The communities assembled at 12°C are the exception. These communities have high
605 diversity within and between communities, even at high taxonomic levels. These patterns are
606 consistent with expectations under a neutral regime (Thompson et al. 2020; Gravel et al. 2006;

607 Vellend 2010) and at this temperature, the difference between functional groups is minimized.
608 Fermenters grow only slightly faster than respirators and secrete little to no organic acids into
609 the media (even after 48hrs of growth).
610
611 Our results demonstrate how physiological and metabolic constraints can be used to
612 predict the effects of environmental factors on community assembly. In this case, two simple
613 metabolic constraints help us predict changes in community assembly along a temperature
614 gradient. First, fermenters grow faster in sugars than respirators, but once they are growing in
615 sugars it takes them a long time to switch strategies and start consuming organic acids (Estrela
616 et al. 2022). Second, increasing the fermenters' growth rates leads to increasing organic acid
617 secretions (Estrela et al. 2022; Basan et al. 2015).
618
619 The first of these constraints seems to result from the underlying metabolic architecture.
620 Sugars and organic acids get catabolized by the central metabolism, using opposite directions
621 of the same metabolic pathways. This metabolic structure restricts the co-utilization of organic
622 acids and sugars leading to conflicts between pathways and potential futile cycles. This
623 metabolic architecture imposes a trade-off between growth rates on one kind of carbon source
624 and the time required to switch metabolic pathways (Schink et al. 2022; Basan et al. 2020), and
625 could have favored the evolution of specialist taxa (e.g. fermenters vs. respirators). In
626 particular, fermenter (glycolytic) taxa grow fast in sugars but have a long lag time between
627 exhausting the sugar and before they can grow on available organic acids (Basan et al. 2020;
628 Schink et al. 2022). Specialization along this axis seems to play an important role in structuring
629 different microbial communities. In a recent study, for example, researchers found that most
630 of the variation between metabolic preferences of isolates from marine heterotrophic bacterial
631 communities was explained by an axis of sugars to organic acids preference (Gralka, Pollak,
632 and Cordero 2022). In our system, this preference underpins a clear distinction between
633 communities assembled in sugars or in organic acids (Estrela et al. 2021).
634

635 The second of these constraints (i.e. faster growth of fermenters is associated with
636 increasing organic acid secretions) comes from previous observations of growth dependency
637 of overflow metabolism (the production of seemingly wasteful by-products during growth on
638 glycolytic substrates even in the presence of oxygen, when full respiration would be more
639 efficient) (Basan et al. 2015; Millard et al. 2021; Szenk, Dill, and de Graff 2017). We had
640 previously observed this relationship between growth rates and overflow metabolism across
641 fermenter species in our system when grown at 30° but we did not know if this relationship
642 would be maintained across temperatures.
643
644 It has been proposed that overflow metabolism increases with growth rates due to
645 increasing proteome limitation (fermentation is less efficient in terms of energy conversion but
646 it is cheaper in terms of proteome use) (Basan et al. 2015). In conflict with our results, these
647 models predict that increased translational efficiency at higher temperatures compensates for
648 the demands of faster growth, maintaining the same levels of overflow metabolism along a
649 broad range of temperatures (Mairet, Gouzé, and de Jong 2021) . Here we show an increase
650 in organic acid secretion with increasing temperatures, and, except for isolates growing past
651 their T_{opt}, all temperatures fall along the same line.
652
653 There are multiple possible reasons for this discrepancy between theoretical
654 predictions and our observations. First, there are other possible mechanisms predicting
655 overflow metabolism, all based on growth constraints (de Groot et al. 2020). Second, while our
656 environments cannot be fully oxygen limited or we would not see growth of respirators, our
657 media is never shaken and therefore there is spatial and temporal variability in oxygen
658 availability. In addition, changes in temperature affect rates of oxygen consumption and
659 oxygen solubility, potentially affecting the metabolic strategies of fermenters. A better
660 understanding of overflow metabolism requires studying different organisms in a range of
661 environmental conditions. As such, not only can physiological studies provide insight into
662 ecology, but a better understanding of microbial ecology and evolution can provide insight
663 into bacterial physiology.

Finally, this study demonstrates the importance of considering metabolic plasticity, and different metabolic strategies when trying to understand the thermal responses of microbial communities. Bacteria are able to change their metabolic strategies in response to environmental conditions and changing constraints (Basan et al. 2015). For instance, microbes can decrease their investment in biomass to cope with increased maintenance costs under stress conditions (Malik et al. 2020). With increasing temperatures, cells will experience protein unfolding-related stress (Richter et al. 2010) which (at very high temperatures) will stimulate cell allocation towards less biomass investment (Mairet, Gouzé, and de Jong 2021). Even before unfolding related stress sinks in, it has been hypothesized that at higher temperatures carbon use efficiency (CUE) should decrease due to higher thermal sensitivity of catabolism than growth (Allison 2014; Manzoni et al. 2012; Ye et al. 2020). However, the evidence is mixed at population and community levels (Frey et al. 2013; Ye et al. 2019; T. P. Smith et al. 2021). Our work suggests that part of the answer might be related to the expression of different metabolic strategies in response to increasing temperatures and changing carbon sources.

Consistent with these observations, long-term warming experiments suggest that changes in dominant carbon sources might have affected the carbon use efficiency of microbial communities in the warming treatment (Melillo et al. 2017). Similarly, a meta-analysis showed variation in CUE with carbon source additions, demonstrating a significant difference between organic acids (excluding amino acids) and glucose (Qiao et al. 2019). These studies highlight the need for systematic physiological descriptions and the development of theories that integrate information from cells into communities and ecosystem processes.

Long-term changes of microbial communities in response to climate change in natural ecosystems such as soil are more complex than our communities assembled in synthetic habitats. However, the relatively simple conditions in the lab make it possible to control and monitor community assembly under different conditions, resulting in a mechanistic understanding of their response to focal environmental factors (Estrela, Sánchez, and

Rebolleda-Gómez 2021; Sun and Sanchez 2023). Ecological forecasting is a challenging task. Even the integration of more detailed physiological descriptions remains a challenge. First, we require a better understanding of how physiological changes at the organismal level can affect species interactions. Second, it would be intractable to incorporate detailed physiological information for all species and interactions. Instead, in this paper, we use broad functional responses and general trade-offs to increase our predictability.

These communities can potentially serve as representations of some simple environments, but their main role is to illuminate important processes potentially affecting community structure and function. These simple replicated communities represent a proof-of-principle that a better understanding of bacterial metabolism and physiology can provide simple rules to predict changes in community composition in response to abiotic changes.

Data and Code Availability

All data and code are available on a repository on GitHub (https://github.com/mrebolleda/TemperatureCommunities).

References

Abreu, Clare I., Martina Dal Bello, Carina Bunse, Jarone Pinhassi, and Jeff Gore. 2023. "Warmer Temperatures Favor Slower-Growing Bacteria in Natural Marine Communities." *Science Advances* 9 (19): eade8352.

Albright, Michaeline B. N., Alexander B. Chase, and Jennifer B. H. Martiny. 2019. "Experimental Evidence That Stochasticity Contributes to Bacterial Composition and Functioning in a Decomposer Community." *mBio* 10 (2). https://doi.org/10.1128/mBio.00568-19.

Allison, Steven D. 2014. "Modeling Adaptation of Carbon Use Efficiency in Microbial Communities." *Frontiers in Microbiology* 5 (October): 571.

Allison, Steven D., Adriana L. Romero-Olivares, Ying Lu, John W. Taylor, and Kathleen K. Treseder. 2018. "Temperature Sensitivities of Extracellular Enzyme Vmax and Km across Thermal Environments." *Global Change Biology* 24 (7): 2884–97.

Allison, Steven D., Matthew D. Wallenstein, and Mark A. Bradford. 2010. "Soil-Carbon Response to Warming Dependent on Microbial Physiology." *Nature Geoscience* 3 (5): 336–40.

Amarasekare, Priyanga. 2015. "Effects of Temperature on Consumer-Resource Interactions." *The Journal of Animal Ecology* 84 (3): 665–79.

Auffret, Marc D., Kristiina Karhu, Amit Khachane, Jennifer A. J. Dungait, Fiona Fraser, David W. Hopkins, Philip A. Wookey, et al. 2016. "The Role of Microbial Community Composition in Controlling Soil Respiration Responses to Temperature." *PloS One* 11 (10): e0165448.

Basan, Markus, Tomoya Honda, Dimitris Christodoulou, Manuel Hörl, Yu-Fang Chang, Emanuele Leoncini, Avik Mukherjee, et al. 2020. "A Universal Trade-off between Growth and Lag in Fluctuating Environments." *Nature* 584 (7821): 470–74.

Basan, Markus, Sheng Hui, Hiroyuki Okano, Zhongge Zhang, Yang Shen, James R. Williamson, and Terence Hwa. 2015. "Overflow Metabolism in Escherichia Coli Results from Efficient Proteome Allocation." *Nature* 528 (7580): 99–104.

Brown, James H., James F. Gillooly, Andrew P. Allen, Van M. Savage, and Geoffrey B. West. 2004. "Toward a Metabolic Theory of Ecology." *Ecology* 85 (7): 1771–89.

Burke, Catherine, Peter Steinberg, Doug Rusch, Staffan Kjelleberg, and Torsten Thomas. 2011. "Bacterial Community Assembly Based on Functional Genes rather than Species." *Proceedings of the National Academy of Sciences of the United States of America* 108 (34): 14288–93.

Burnside, William R., Erik B. Erhardt, Sean T. Hammond, and James H. Brown. 2014. "Rates of Biotic Interactions Scale Predictably with Temperature despite Variation." *Oikos* 123 (12): 1449–56.

Callahan, Benjamin J., Paul J. McMurdie, Michael J. Rosen, Andrew W. Han, Amy Jo A. Johnson, and Susan P. Holmes. 2016. "DADA2: High-Resolution Sample Inference from Illumina Amplicon Data." *Nature Methods* 13 (7): 581–83.

Caporaso, J. Gregory, Christian L. Lauber, William A. Walters, Donna Berg-Lyons, James Huntley, Noah Fierer, Sarah M. Owens, et al. 2012. "Ultra-High-Throughput Microbial Community Analysis on the Illumina HiSeq and MiSeq Platforms." *The ISME Journal* 6 (8): 1621–24.

Cavigelli, Michel A., and G. Philip Robertson. 2000. "The Functional Significance of Denitrifier Community Composition in a Terrestrial Ecosystem." *Ecology* 81 (5): 1402–14.

Chappell, Callie R., Manpreet K. Dhami, Mark C. Bitter, Lucas Czech, Sur Herrera Paredes, Fatoumata Binta Barrie, Yadira Calderón, et al. 2022. "Wide-Ranging Consequences of Priority Effects Governed by an Overarching Factor." *eLife* 11 (October). https://doi.org/10.7554/eLife.79647.

Crocker, Kyle, Milena Chakraverti-Wuerthwein, Zeqian Li, Madhav Mani, Karna Gowda, and Seppe Kuehn. 2023. "Genomic Patterns in the Global Soil Microbiome Emerge from Microbial Interactions." *bioRxiv*. https://doi.org/10.1101/2023.05.31.542950.

Davidson, Eric A., and Ivan A. Janssens. 2006. "Temperature Sensitivity of Soil Carbon Decomposition and Feedbacks to Climate Change." *Nature* 440 (7081): 165–73.

DeAngelis, Kristen M., Grace Pold, Begüm D. Topçuoğlu, Linda T. A. van Diepen, Rebecca M. Varney, Jeffrey L. Blanchard, Jerry Melillo, and Serita D. Frey. 2015. "Long-Term Forest

Soil Warming Alters Microbial Communities in Temperate Forest Soils." *Frontiers in Microbiology* 6 (February): 104.

Debray, Reena, Robin A. Herbert, Alexander L. Jaffe, Alexander Crits-Christoph, Mary E. Power, and Britt Koskella. 2022. "Priority Effects in Microbiome Assembly." *Nature Reviews. Microbiology* 20 (2): 109–21.

Dell, Anthony I., Samraat Pawar, and Van M. Savage. 2014. "Temperature Dependence of Trophic Interactions Are Driven by Asymmetry of Species Responses and Foraging Strategy." *The Journal of Animal Ecology* 83 (1): 70–84.

Dziallas, Claudia, and Hans-Peter Grossart. 2012. "Microbial Interactions with the Cyanobacterium Microcystis Aeruginosa and Their Dependence on Temperature." *Marine Biology* 159 (11): 2389–98.

Estrela, Sylvie, Álvaro Sánchez, and María Rebolleda-Gómez. 2021. "Multi-Replicated Enrichment Communities as a Model System in Microbial Ecology." *Frontiers in Microbiology* 12 (April): 657467.

Estrela, Sylvie, Alicia Sanchez-Gorostiaga, Jean Cc Vila, and Alvaro Sanchez. 2021. "Nutrient Dominance Governs the Assembly of Microbial Communities in Mixed Nutrient Environments." *eLife* 10 (April). https://doi.org/10.7554/eLife.65948.

Estrela, Sylvie, Jean C. C. Vila, Nanxi Lu, Djordje Bajić, Maria Rebolleda-Gómez, Chang-Yu Chang, Joshua E. Goldford, Alicia Sanchez-Gorostiaga, and Álvaro Sánchez. 2022. "Functional Attractors in Microbial Community Assembly." *Cell Systems* 13 (1): 29–42.e7.

Frey, Serita D., Juhwan Lee, Jerry M. Melillo, and Johan Six. 2013. "The Temperature Response of Soil Microbial Efficiency and Its Feedback to Climate." *Nature Climate Change* 3 (4): 395–98.

García, Francisca C., Tom Clegg, Daniel Barrios O'Neill, Ruth Warfield, Samraat Pawar, and Gabriel Yvon-Durocher. 2023. "The Temperature Dependence of Microbial Community Respiration Is Amplified by Changes in Species Interactions." *Nature Microbiology* 8 (2): 272–83.

Glassman, Sydney I., Claudia Weihe, Junhui Li, Michaeline B. N. Albright, Caitlin I. Looby, Adam C. Martiny, Kathleen K. Treseder, Steven D. Allison, and Jennifer B. H. Martiny.

2018. "Decomposition Responses to Climate Depend on Microbial Community Composition." *Proceedings of the National Academy of Sciences of the United States of America* 115 (47): 11994–99.

Goldford, Joshua E., Nanxi Lu, Djordje Bajić, Sylvie Estrela, Mikhail Tikhonov, Alicia Sanchez-Gorostiaga, Daniel Segrè, Pankaj Mehta, and Alvaro Sanchez. 2018. "Emergent Simplicity in Microbial Community Assembly." *Science* 361 (6401): 469–74.

Goldsby, Heather J., Anna Dornhaus, Benjamin Kerr, and Charles Ofria. 2012. "Task-Switching Costs Promote the Evolution of Division of Labor and Shifts in Individuality." *Proceedings of the National Academy of Sciences of the United States of America* 109 (34): 13686–91.

Gralka, Matti, Shaul Pollak, and Otto X. Cordero. 2022. "Fundamental Metabolic Strategies of Heterotrophic Bacteria." *bioRxiv*. https://doi.org/10.1101/2022.08.04.502823.

Gravel, Dominique, Charles D. Canham, Marilou Beaudet, and Christian Messier. 2006. "Reconciling Niche and Neutrality: The Continuum Hypothesis." *Ecology Letters* 9 (4): 399–409.

Groot, Daan H. de, Julia Lischke, Riccardo Muolo, Robert Planqué, Frank J. Bruggeman, and Bas Teusink. 2020. "The Common Message of Constraint-Based Optimization Approaches: Overflow Metabolism Is Caused by Two Growth-Limiting Constraints." *Cellular and Molecular Life Sciences: CMLS* 77 (3): 441–53.

Hall, E. K., and J. B. Cotner. 2007. "Interactive Effect of Temperature and Resources on Carbon Cycling by Freshwater Bacterioplankton Communities." *Aquatic Microbial Ecology: International Journal* 49 (October): 35–45.

Kim, Heather H., Charlotte Laufkötter, Tomas Lovato, Scott C. Doney, and Hugh W. Ducklow. 2023. "Projected 21st-Century Changes in Marine Heterotrophic Bacteria under Climate Change." *Frontiers in Microbiology* 14 (February): 1049579.

Louca, Stilianos, Laura Wegener Parfrey, and Michael Doebeli. 2016. "Decoupling Function and Taxonomy in the Global Ocean Microbiome." *Science* 353 (6305): 1272–77.

Louca, Stilianos, Martin F. Polz, Florent Mazel, Michaeline B. N. Albright, Julie A. Huber, Mary I. O'Connor, Martin Ackermann, et al. 2018. "Function and Functional Redundancy in

Microbial Systems." *Nature Ecology & Evolution* 2 (6): 936–43.

Lynch, Michael, and Wilfried Gabriel. 1987. "Environmental Tolerance." *The American Naturalist* 129 (2): 283–303.

Mairet, Francis, Jean-Luc Gouzé, and Hidde de Jong. 2021. "Optimal Proteome Allocation and the Temperature Dependence of Microbial Growth Laws." *NPJ Systems Biology and Applications* 7 (1): 14.

Malik, Ashish A., Tami Swenson, Claudia Weihe, Eric W. Morrison, Jennifer B. H. Martiny, Eoin L. Brodie, Trent R. Northen, and Steven D. Allison. 2020. "Drought and Plant Litter Chemistry Alter Microbial Gene Expression and Metabolite Production." *The ISME Journal* 14 (9): 2236–47.

Manzoni, Stefano, Philip Taylor, Andreas Richter, Amilcare Porporato, and Göran I. Ågren. 2012. "Environmental and Stoichiometric Controls on Microbial Carbon-Use Efficiency in Soils." *The New Phytologist* 196 (1): 79–91.

Matulich, Kristin L., and Jennifer B. H. Martiny. 2015. "Microbial Composition Alters the Response of Litter Decomposition to Environmental Change." *Ecology* 96 (1): 154–63.

Melillo, J. M., S. D. Frey, K. M. DeAngelis, W. J. Werner, M. J. Bernard, F. P. Bowles, G. Pold, M. A. Knorr, and A. S. Grandy. 2017. "Long-Term Pattern and Magnitude of Soil Carbon Feedback to the Climate System in a Warming World." *Science* 358 (6359): 101–5.

Millard, Pierre, Brice Enjalbert, Sandrine Uttenweiler-Joseph, Jean-Charles Portais, and Fabien Létisse. 2021. "Control and Regulation of Acetate Overflow in Escherichia Coli." *eLife* 10 (March). https://doi.org/10.7554/eLife.63661.

Nelson, Michaeline B., Adam C. Martiny, and Jennifer B. H. Martiny. 2016. "Global Biogeography of Microbial Nitrogen-Cycling Traits in Soil." *Proceedings of the National Academy of Sciences of the United States of America* 113 (29): 8033–40.

Nguyen, Trang T. H., Emily J. Zakem, Ali Ebrahimi, Julia Schwartzman, Tolga Caglar, Kapil Amarnath, Uria Alcolombri, et al. 2022. "Microbes Contribute to Setting the Ocean Carbon Flux by Altering the Fate of Sinking Particulates." *Nature Communications* 13 (1): 1657.

Oksanen, Jari, Roeland Kindt, Pierre Legendre, Bob O'Hara, M. Henry H. Stevens, Maintainer

Jari Oksanen, and Mass Suggests. 2007. "The Vegan Package." *Community Ecology Package* 10 (631-637): 719.

Padfield, Daniel, Hannah O'Sullivan, and Samraat Pawar. 2021. "rTPC and Nls.multstart : A New Pipeline to Fit Thermal Performance Curves in R." *Methods in Ecology and Evolution / British Ecological Society* 12 (6): 1138–43.

Pfeiffer, Thomas, and Sebastian Bonhoeffer. 2002. "Evolutionary Consequences of Tradeoffs between Yield and Rate of ATP Production" 216 (1): 51.

Pfeiffer, T., S. Schuster, and S. Bonhoeffer. 2001. "Cooperation and Competition in the Evolution of ATP-Producing Pathways." *Science* 292 (5516): 504–7.

Pontrelli, Sammy, Rachel Szabo, Shaul Pollak, Julia Schwartzman, Daniela Ledezma-Tejeida, Otto X. Cordero, and Uwe Sauer. 2022. "Metabolic Cross-Feeding Structures the Assembly of Polysaccharide Degrading Communities." *Science Advances* 8 (8): eabk3076.

Postmus, Jarne, André B. Canelas, Jildau Bouwman, Barbara M. Bakker, Walter van Gulik, M. Joost Teixeira de Mattos, Stanley Brul, and Gertien J. Smits. 2008. "Quantitative Analysis of the High Temperature-Induced Glycolytic Flux Increase in Saccharomyces Cerevisiae Reveals Dominant Metabolic Regulation." *The Journal of Biological Chemistry* 283 (35): 23524–32.

Price, P. Buford, and Todd Sowers. 2004. "Temperature Dependence of Metabolic Rates for Microbial Growth, Maintenance, and Survival." *Proceedings of the National Academy of Sciences of the United States of America* 101 (13): 4631–36.

Qiao, Yang, Jing Wang, Guopeng Liang, Zhenggang Du, Jian Zhou, Chen Zhu, Kun Huang, et al. 2019. "Global Variation of Soil Microbial Carbon-Use Efficiency in Relation to Growth Temperature and Substrate Supply." *Scientific Reports* 9 (1): 5621.

R Core Team. 2023. "R: A Language and Environment for Statistical Computing." Vienna, Austria: R Foundation for Statistical Computing. https://www.R-project.org/.

Reed, Heather E., and Jennifer B. H. Martiny. 2013. "Microbial Composition Affects the Functioning of Estuarine Sediments." *The ISME Journal* 7 (4): 868–79.

Savage, Van M., James F. Gillooly, James H. Brown, Geoffrey B. West, and Eric L. Charnov.

2004. "Effects of Body Size and Temperature on Population Growth." *The American Naturalist* 163 (3): 429–41.

Schink, Severin Josef, Dimitris Christodoulou, Avik Mukherjee, Edward Athaide, Viktoria Brunner, Tobias Fuhrer, Gary Andrew Bradshaw, Uwe Sauer, and Markus Basan. 2022. "Glycolysis/gluconeogenesis Specialization in Microbes Is Driven by Biochemical Constraints of Flux Sensing." *Molecular Systems Biology* 18 (1): e10704.

Schlesinger, William H., and Jeffrey A. Andrews. 2000. "Soil Respiration and the Global Carbon Cycle." *Biogeochemistry* 48 (1): 7–20.

Sheik, Cody S., William Howard Beasley, Mostafa S. Elshahed, Xuhui Zhou, Yiqi Luo, and Lee R. Krumholz. 2011. "Effect of Warming and Drought on Grassland Microbial Communities." *The ISME Journal* 5 (10): 1692–1700.

Smith, Daniel J., and Priyanga Amarasekare. 2018. "Toward a Mechanistic Understanding of Thermal Niche Partitioning." *The American Naturalist* 191 (3): E57–75.

Smith, Thomas P., Tom Clegg, Thomas Bell, and Samrāt Pawar. 2021. "Systematic Variation in the Temperature Dependence of Bacterial Carbon Use Efficiency." *Ecology Letters* 24 (10): 2123–33.

Solden, Lindsey M., Adrian E. Naas, Simon Roux, Rebecca A. Daly, William B. Collins, Carrie D. Nicora, Sam O. Purvine, et al. 2018. "Interspecies Cross-Feeding Orchestrates Carbon Degradation in the Rumen Ecosystem." *Nature Microbiology* 3 (11): 1274–84.

Suding, Katharine N., Katherine L. Gross, and Gregory R. Houseman. 2004. "Alternative States and Positive Feedbacks in Restoration Ecology." *Trends in Ecology & Evolution* 19 (1): 46–53.

Sun, Xin, and Alvaro Sanchez. 2023. "Synthesizing Microbial Biodiversity." *Current Opinion in Microbiology* 75 (October): 102348.

Szenk, Mariola, Ken A. Dill, and Adam M. R. de Graff. 2017. "Why Do Fast-Growing Bacteria Enter Overflow Metabolism? Testing the Membrane Real Estate Hypothesis." *Cell Systems* 5 (2): 95–104.

Thomas, Mridul K., Colin T. Kremer, Christopher A. Klausmeier, and Elena Litchman. 2012. "A Global Pattern of Thermal Adaptation in Marine Phytoplankton." *Science* 338 (6110):

1085–88.

Thompson, Patrick L., Laura Melissa Guzman, Luc De Meester, Zsófia Horváth, Robert Ptacnik, Bram Vanschoenwinkel, Duarte S. Viana, and Jonathan M. Chase. 2020. "A Process-Based Metacommunity Framework Linking Local and Regional Scale Community Ecology." *Ecology Letters* 23 (9): 1314–29.

Tseng, M., Joey R. Bernhardt, and Alexander E. Chila. 2019. "Species Interactions Mediate Thermal Evolution." *Evolutionary Applications* 12 (7): 1463–74.

Vellend, Mark. 2010. "Conceptual Synthesis in Community Ecology." *The Quarterly Review of Biology* 85 (2): 183–206.

Wang, Qiong, George M. Garrity, James M. Tiedje, and James R. Cole. 2007. "Naive Bayesian Classifier for Rapid Assignment of rRNA Sequences into the New Bacterial Taxonomy." *Applied and Environmental Microbiology* 73 (16): 5261–67.

Wood, Simon N. 2011. "Fast Stable Restricted Maximum Likelihood and Marginal Likelihood Estimation of Semiparametric Generalized Linear Models." *Journal of the Royal Statistical Society. Series B, Statistical Methodology* 73 (1): 3–36.

Wu, Linwei, Ya Zhang, Xue Guo, Daliang Ning, Xishu Zhou, Jiajie Feng, Mengting Maggie Yuan, et al. 2022. "Reduction of Microbial Diversity in Grassland Soil Is Driven by Long-Term Climate Warming." *Nature Microbiology* 7 (7): 1054–62.

Xiao, Xian, Manuel Delgado-Baquerizo, Haoyang Shen, Zhiyuan Ma, Jizhong Zhou, Bo Sun, and Yuting Liang. 2023. "Microbial Interactions Related to N2O Emissions and Temperature Sensitivity from Rice Paddy Fields." *mBio* 14 (1): e0326222.

Ye, Jian-Sheng, Mark A. Bradford, Marina Dacal, Fernando T. Maestre, and Pablo García-Palacios. 2019. "Increasing Microbial Carbon Use Efficiency with Warming Predicts Soil Heterotrophic Respiration Globally." *Global Change Biology* 25 (10): 3354–64.

Ye, Jian-Sheng, Mark A. Bradford, Fernando T. Maestre, Feng-Min Li, and Pablo García-Palacios. 2020. "Compensatory Thermal Adaptation of Soil Microbial Respiration Rates in Global Croplands." *Global Biogeochemical Cycles* 34 (6). https://doi.org/10.1029/2019gb006507.